TECHNICAL REPORT ARBRL-TR-02384

COMPUTATIONS OF THE MAGNUS EFFECT FOR SLENDER BODIES IN SUPERSONIC FLOW

Walter B. Sturek
Lewis B. Schiff

December 1981

US ARMY ARMAMENT RESEARCH AND DEVELOPMENT COMMAND
BALLISTIC RESEARCH LABORATORY
ABERDEEN PROVING GROUND, MARYLAND

Destroy this report when it is no longer needed.
Do not return it to the originator.

Secondary distribution of this report by originating or sponsoring activity is prohibited.

Additional copies of this report may be obtained from the National Technical Information Service, U.S. Department of Commerce, Springfield, Virginia 22161.

The findings in this report are not to be construed as an official Department of the Army position, unless so designated by other authorized documents.

The use of trade names or manufacturers' names in this report does not constitute indorsement of any commercial product.

UNCLASSIFIED

SECURITY CLASSIFICATION OF THIS PAGE *(When Data Entered)*

REPORT DOCUMENTATION PAGE		READ INSTRUCTIONS BEFORE COMPLETING FORM
1. REPORT NUMBER TECHNICAL REPORT ARBRL-TR-02384	2. GOVT ACCESSION NO.	3. RECIPIENT'S CATALOG NUMBER
4. TITLE *(and Subtitle)* COMPUTATIONS OF THE MAGNUS EFFECT FOR SLENDER BODIES IN SUPERSONIC FLOW		5. TYPE OF REPORT & PERIOD COVERED Final 6. PERFORMING ORG. REPORT NUMBER
7. AUTHOR(s) Walter B. Sturek and Lewis B. Schiff, NASA Ames Research Center		8. CONTRACT OR GRANT NUMBER(s)
9. PERFORMING ORGANIZATION NAME AND ADDRESS U.S. Army Ballistic Research Laboratory (ATTN: DRDAR-BLL) Aberdeen Proving Ground, Maryland 21005		10. PROGRAM ELEMENT, PROJECT, TASK AREA & WORK UNIT NUMBERS RDT&E 1L162618AH80
11. CONTROLLING OFFICE NAME AND ADDRESS US Army Armament Research & Development Command US Army Ballistic Research Laboratory (DRDAR-BL) Aberdeen Proving Ground, MD 21005		12. REPORT DATE December 1981 13. NUMBER OF PAGES 41
14. MONITORING AGENCY NAME & ADDRESS*(If different from Controlling Office)*		15. SECURITY CLASS. *(of this report)* Unclassified 15a. DECLASSIFICATION/DOWNGRADING SCHEDULE

16. DISTRIBUTION STATEMENT *(of this Report)*

Approved for public release; distribution unlimited.

17. DISTRIBUTION STATEMENT *(of the abstract entered in Block 20, if different from Report)*

18. SUPPLEMENTARY NOTES

19. KEY WORDS *(Continue on reverse side if necessary and identify by block number)*

Turbulent Boundary Layer
Navier-Stokes Computations
Magnus Effect
Supersonic Flow

20. ABSTRACT *(Continue on reverse side if necessary and identify by block number)*

A recently reported Parabolized Navier-Stokes code has been employed to compute the supersonic flow field about spinning cone, ogive-cylinder, and boattailed bodies of revolution at moderate incidence. The computations were performed for flow conditions where extensive measurements for wall pressure, boundary-layer velocity profiles and Magnus force had been obtained. Comparisons between the computational results and experiment indicate excellent agreement for angles of attack up to 6°. The comparisons for Magnus effects show that the code accurately predicts the effects of body shape and

DD FORM 1 JAN 73 1473 EDITION OF 1 NOV 65 IS OBSOLETE

UNCLASSIFIED

SECURITY CLASSIFICATION OF THIS PAGE *(When Data Entered)*

20. ABSTRACT (Continued)

Mach number for the selected models for $2 \leq M \leq 4$.

TABLE OF CONTENTS

LIST OF ILLUSTRATIONS

LIST OF ILLUSTRATIONS
(Continued)

LIST OF TABLES

I. INTRODUCTION

The use of separate codes for computing inviscid flow and turbulent boundary layer development over yawed, spinning and non-spinning bodies of revolution has yielded some very good solutions for cone and ogive-cylinder shapes[1]. However, the authors of Reference 1 have found that application of these techniques to bodies with boattailed afterbodies has not yielded satisfactory results even at small angles of attack ($\alpha \leq 4°$).

Several recent publications have reported supersonic flow field computations using Parabolized Navier-Stokes (PNS) techniques. These publications have reported very good results for cone models for laminar and turbulent viscous flow[2,3], and for cone and ogive-cylinder models for laminar viscous flow[4,5]. The PNS method appears to offer an attractive technique for computing flow over bodies with discontinuities in surface curvature (such as occurs at the junction between the cylinder and the boattail) since the inviscid flow and viscous layer are computed simultaneously. Further, the PNS method permits adequate flow field resolution to be achieved with very reasonable computer costs. This report documents detailed comparisons of PNS computational results to experimental measurements of turbulent boundary layer profile characteristics of a spinning ogive-cylinder-boattail body at Mach = 3. In addition, comparisons are made between the PNS computations, boundary layer-inviscid computations, and experimental measurements of Magnus forces for cone, ogive-cylinder, and ogive-cylinder-boattail models for $2 \leq M \leq 4$. The PNS code is that reported by Schiff and Steger[6]. The boundary layer-inviscid code is that reported by Sturek, et al[1].

---

1. *Sturek, W.B., Dwyer, H.A., Kayser, L.D., Nietubicz, C.J., Reklis, R.P., and Opalka, K.O., "Computations of Magnus Effects for a Yawed, Spinning Body of Revolution," AIAA Journal, Vol. 16, No. 7, July 1978, pp. 687-692.*

2. *Lin, T. C., and Rubin, S. G., "Viscous Flow Over a Cone at Moderate Incidence: I Hypersonic Tip Region", Computers and Fluids, Vol. 1, 1973, pp. 37-57.*

3. *Lubard, S. C., and Helliwell, W. S., "Calculation of the Flow on a Cone at High Angle of Attack", AIAA Journal, Vol. 12, July 1974, pp. 965-974.*

4. *Rakich, J. V., Vigneron, Y. C., and Agarwal, R., "Computation of Supersonic Viscous Flows Over Ogive-Cylinders at Angle of Attack", AIAA Paper No. 79-0131, 17th Aerospace Sciences Meeting, January 1979.*

5. *Agarwal, R., and Rakich, J. V., "Computation of Hypersonic Laminar Viscous Flow Past Spinning Sharp and Blunt Cones at High Angle of Attack", AIAA Paper No. 78-65, AIAA 16th Aerospace Sciences Meeting, January 1978.*

6. *Schiff, L. B., and Steger, J.L., "Numerical Simulation of Steady Supersonic Viscous Flow", AIAA Journal, Vol. 18, No. 12, December 1980, pp. 1421-1430.*

II. OVERVIEW OF NUMERICAL SCHEME

A. Governing Equations and Numerical Scheme

A body-conforming ξ, η, ζ, coordinate system (Figure 1) is used which maps the body surface and outer boundary of the flow region in physical space onto coordinate surfaces of the computational space. This transformation simplifies the application of surface boundary conditions and permits the approximation of neglecting streamwise and circumferential viscous terms in high-Reynolds-number flow (see Ref. 6). The resulting steady thin-layer PNS equations can be written in strong conservation-law form in terms of nondimensional variables as

$$\frac{\partial \hat{E}_s}{\partial \xi} + \frac{\partial \hat{F}}{\partial \eta} + \frac{\partial \hat{G}}{\partial \zeta} = \frac{1}{\hat{Re}} \frac{\partial \hat{S}}{\partial \zeta} \tag{1}$$

where

$\xi = \xi(x)$ is the axial (marching) coordinate

$\eta = \eta(x,y,z)$ is the circumferential coordinate

$\zeta = \zeta(x,y,z)$ is the normal coordinate

The inviscid flux vectors in Eq. (1) are

$$E_s = J^{-1} \begin{bmatrix} \rho U \\ \rho uU + \xi_x p \\ \rho vU \\ \rho wU \\ (e+p_s)U \end{bmatrix}, \quad F = J^{-1} \begin{bmatrix} \rho V \\ \rho uV + \eta_x p \\ \rho vV + \eta_y p \\ \rho wV + \eta_z p \\ (e+p)V \end{bmatrix}, \quad G = J^{-1} \begin{bmatrix} \rho W \\ \rho uW + \zeta_x p \\ \rho vW + \zeta_y p \\ \rho wW + \zeta_z p \\ (e+p)W \end{bmatrix} \tag{2}$$

with contravariant velocity components

$$\left.\begin{aligned} U &= \xi_x u \\ V &= \eta_x u + \eta_y v + \eta_z w \\ W &= \zeta_x u + \zeta_y v + \zeta_z w \end{aligned}\right\} \tag{3}$$

The internal energy of the gas e_i is defined in terms of the conservative variables as

$$e_i = (e/\rho) - 0.5(u^2 + v^2 + w^2) \tag{4}$$

while the equation of state for a perfect gas with ratio of specific heats γ is

$$p/\rho = (\gamma - 1)e_i = a^2/\gamma \tag{5}$$

Variations of body geometry are included in Eq. (1) through the presence of the metric terms ξ_x, η_x, η_y, etc., which appear in the flux vectors. The thin-layer viscous terms, valid for high-Reynolds-number flow, are

$$\hat{S} = J^{-1}\begin{bmatrix} 0 \\ \mu(\zeta_x^2+\zeta_y^2+\zeta_z^2)u_\zeta + (\mu/3)(\zeta_x u_\zeta+\zeta_y v_\zeta+\zeta_z w_\zeta)\zeta_x \\ \mu(\zeta_x^2+\zeta_y^2+\zeta_z^2)v_\zeta + (\mu/3)(\zeta_x u_\zeta+\zeta_y v_\zeta+\zeta_z w_\zeta)\zeta_y \\ \mu(\zeta_x^2+\zeta_y^2+\zeta_z^2)w_\zeta + (\mu/3)(\zeta_x u_\zeta+\zeta_y v_\zeta+\zeta_z w_\zeta)\zeta_z \\ \{(\zeta_x^2+\zeta_y^2+\zeta_z^2)[(\mu/2)(u^2+v^2+w^2)_\zeta \\ + \kappa Pr^{-1}(\gamma-1)^{-1}(a^2)_\zeta] + (\mu/3)(\zeta_x u \\ + \zeta_y v + \zeta_z w)(\zeta_x u_\zeta + \zeta_y v_\zeta + \zeta_z w_\zeta)\} \end{bmatrix} \tag{6}$$

Equation (1) is parabolic with respect to ξ and can thus be marched downstream in the ξ direction from an initial data plane (subject to appropriate body and free-stream boundary conditions) under those conditions where the local flow is supersonic. By evaluating the pressure, p_s, in the $\hat{E}_s$ flux vector using the subsonic layer approximation, Eq. (1) can be kept stable for marching for subsonic points as well. When p_s is set equal to the local pressure for supersonic points, and is evaluated from $\partial p_s/\partial\zeta = 0$ (Figure 2) for points within the subsonic viscous layer adjacent to a wall, Eq. (1) can be marched stably for all flows where $U > 0$; that is, for flows without streamwise reversal.

The numerical algorithm used to march Eq. (1) downstream is an approximately-factored, fully implicit, finite-difference scheme. The algorithm can be written in so-called delta form as

$$
\begin{aligned}
&[\tilde{A}_s^{\,j} + (1-\alpha)\Delta\xi(\delta_\eta \tilde{B}^j)](\tilde{A}_s^{\,j})^{-1} \\
&\times [\tilde{A}_s^{\,j} + (1-\alpha)\Delta\xi(\delta_\zeta \tilde{C}^j - \hat{Re}^{-1}\,\bar{\delta}_\zeta \tilde{M}^j)]\Delta\hat{q}^j \\
&= -(\tilde{A}_s^{\,j} - \tilde{A}_s^{j-1})\hat{q}^j + \alpha(\hat{E}_s^{\,j} - \hat{E}_s^{j-1}) \\
&- (1-\alpha)\Delta\xi\{\delta_\eta[\eta_x^{j+1}(E/J)^j + \eta_y^{j+1}(F/J)^j + \eta_z^{j+1}(G/J)^j] \\
&\quad + \delta_\zeta[\zeta_x^{j+1}(E/J)^j + \zeta_y^{j+1}(F/J)^j + \zeta_z^{j+1}(G/J)^j] \\
&\quad - \hat{Re}^{-1}\bar{\delta}_\zeta \tilde{S}^j\} - [(\xi_x/J)^{j+1}E_p^{\,j} - (\xi_x/J)^j E_p^{j-1}] + \mathcal{D}\hat{q}^j
\end{aligned}
\qquad (7)
$$

where $\hat{q} = J^{-1}\,(\rho,\ \rho u,\ \rho v,\ \rho w,\ e)$.

The δ's represent second order central difference operators while Δ represents a conventional forward difference. The Jacobian matrices A, B, and C are defined as $\frac{\partial E}{\partial q}$, $\frac{\partial F}{\partial q}$, and $\frac{\partial G}{\partial q}$, respectively. The coefficient matrix M is obtained from the Taylor series linearization of the viscous vector S. The algorithm shown in Eq. (7) is second order accurate in ξ for $\alpha = 1/3$, and is first order accurate in ξ for $\alpha = 0$. The fourth order dissipation term is represented by $\mathcal{D}$ which is added to damp high-frequency oscillations.

The algorithm is conservative and of second-order accuracy in the marching direction. A two-layer, Cebeci-type eddy viscosity model[7] is included for the computation of turbulent flows. The algorithm has been applied to compute a variety of laminar and turbulent flows and the results have been in excellent agreement with those obtained from more costly time-dependent computations. Full details of the Parabolized Navier-Stokes assumption, and of the derivation of the algorithm are included in Reference 6.

B. Conical Initial Solutions

In general the initial data plane for the marching method must be supplied from an auxiliary computation. However, when treating the flow over conical or pointed bodies, the marching code can be used to generate its own initial data plane. As outlined in Ref. 6, for inviscid conical flows a

---

7. *Baldwin, B. S., and Lomax, H., "Thin Layer Approximation and Algebraic Model for Separated Turbulent Flows", AIAA Paper No. 78-257, 16th Aerospace Sciences Meeting, January 1978.*

conical grid is selected and the flow variables are initially set to free-stream values. The solution is marched downstream from an initial station and, after each step, the solution is scaled to place it back at the original station. When no change in the flow variables occur with further marching, the variables are constant along rays, and a conical solution has been generated. If the flow variables within the viscous layer can also be assumed to be locally constant along rays, the same procedure can be used to generate viscous conical solutions.

For the ogive-cylinder-boattail computations, the tip of the ogive was replaced with a cone tangent to the ogive at x = 0.267 caliber (1 caliber = 1 model diameter). Conical solutions were generated at that station and used as starting data for the marching code. A small error is made in generating the starting solution for cases with surface spin due to the change in circumferential velocity with longitudinal position. However, this error is small since the stepsize used in the conical initial solution is less than 1% of the distance from the tip to the initial plane. In any event, this error is quickly corrected as the initial solution is marched over the body.

C. Adaptive Grid

An adaptive grid capability was developed for the PNS code in order to maintain adequate resolution of the viscous layer as the solution develops over the full length of the spinning model. This capability was also found to be of importance in maintaining computational stability, particularly for the Mach = 4 computations. The strategy used here was to check for the value of y^+ ($y^+ = \rho_w U_\tau y/\mu_w$; $U_\tau = \sqrt{\tau_w/\rho_w}$) at the first grid node above the model surface and to adjust the grid stretching parameters to maintain this value of y^+ within the desired range, $5 \leq y^+ \leq 10$. This check was made only at the wind and lee sides of the model. The stretching parameter was varied linearly between the extremes determined at the wind and lee sides for grid nodes at circumferential stations off the pitch plane. If the value of y^+ was found to be outside the specified criteria, the stretching parameter was adjusted by 0.5% for the next computational step. Although the adaptive grid technique works well in general, it was found that permitting too great a change in the grid configuration from step to step resulted in the introduction of errors into the computation.

III. RESULTS

A. Model Geometry and Experimental Measurements

The dimensions of the ogive-cylinder-boattail model used for the detailed flow field studies are shown in Figure 3. The model is 6 calibers long with a 1-caliber, 7° boattail, and closely resembles a modern low-drag artillery projectile.

A number of wind-tunnel experiments have been conducted for this model geometry in order to obtain data for comparison to numerical computations. The data acquired include measurements of wall static pressure[8], turbulent boundary-layer velocity profiles[9,10], surface skin friction[9], and flow visualization. The test conditions were M = 3 with a tunnel total pressure of 0.298 MPa and tunnel total temperature of 308°K. These conditions produced a free-stream Reynolds number of 7.3×10^6 based on the model length. The boundary layer was tripped near the tip of the model to produce a reliable turbulent flow. Additionally, aerodynamic force[11,12] measurements were available for 10° cone, ogive-cylinder and ogive-cylinder-boattail shapes at M = 2, 3 and 4. These data include Magnus and pitch plane aerodynamic force and moment coefficients. All tests were performed using SSWT Number One at the U.S. Army Ballistic Research Laboratory. This facility, which is no longer in operation, was a continuous flow tunnel with a flexible plate nozzle. The test section size was 330 x 380mm (13 x 15 in.).

B. Comparison Between Computation and Experiment

Computations were performed for a body having the same geometric shape as the experimental model, and for flow conditions duplicating that of the experiment. Turbulent conical solutions were generated at x = 15.2mm (see Figure 3) and used as initial data for the PNS marching code. The present computations used a grid consisting of 36 circumferential points ($\Delta\phi = 10°$)

---

8. *Reklis, R.P., and Sturek, W.B., "Surface Pressure Measurements on Slender Bodies at Angle of Attack in Supersonic Flow", U.S. Army Ballistic Research Laboratory/ARRADCOM Memorandum Report ARBRL-MR-02876, Aberdeen Proving Ground, MD, November 1978. AD A064097.*

9. *Kayser, L. D., and Sturek, W. B., "Experimental Measurements in the Turbulent Boundary Layer of a Yawed, Spinning Ogive-Cylinder Body of Revolution at Mach 3.0. Part II: Data Tabulation", U.S. Army Ballistic Research Laboratory/ARRADCOM Memorandum Report ARBRL-MR-02813, Aberdeen Proving Ground, MD, March 1978. AD A053458.*

10. *Kayser, L. D., and Sturek, W. B., "Turbulent Boundary Layer Measurements on the Boattail Section of a Yawed, Spinning Projectile Shape at Mach 3.0", U.S. Army Ballistic Research Laboratory/ARRADCOM Memorandum Report ARBRL-MR-02880, Aberdeen Proving Ground, MD, November 1978. AD A065355.*

11. *Sturek, W. B., "Boundary Layer Studies on a Spinning Cone,"U.S. Army Ballistic Research Laboratory/ARRADCOM Report BRL-R-1649, Aberdeen Proving Ground, MD, May 1973. AD 762564.*

12. *Nietubicz, C. J., and Opalka, K., "Supersonic Wind Tunnel Measurements of Static and Magnus Aerodynamic Coefficients for Projectile Shapes with Tangent and Secant Ogive Noses", U.S. Army Ballistic Research Laboratory/ ARRADCOM Memorandum Report ARBRL-MR-02991, Aberdeen Proving Ground, MD, February 1980. AD A083297.*

and 50 points radially between the body and the outer boundary. Computation time on the CDC 7600 computer is 2.3 sec/step with this size grid. A detailed comparison of the PNS computations to these data for a non-spinning model has been accomplished[13]. The comparisons of Ref. 13 showed that the PNS numerical technique, in which the viscous layer and the inviscid flow are computed simultaneously, yields a significantly improved agreement with experimentally measured wall pressures over the agreement obtained with inviscid computations for bodies with discontinuities in surface curvature.

Surface Pressure. The PNS computations are compared to experimental measurements and to inviscid flow computations made using codes based on MacCormack's predictor-corrector technique (Figures 4-5). Longitudinal surface pressure distributions along the windward and leeward rays are shown in Figure 4 for an angle of attack of 6.3°. The PNS computations exhibit better agreement with experiment in the vicinity of the discontinuities in streamwise surface curvature at the ogive-cylinder and cylinder-boattail junctions than the inviscid computations.

Examples of comparisons of circumferential surface pressure distributions are shown for $\alpha = 6.3°$ in Figure 5 at two longitudinal stations; one on the cylinder portion of the model near the boattail, the second, midway on the boattail. The comparison on the cylinder indicates excellent agreement between the PNS computation and experiment and the appearance of a systematic discrepancy between the inviscid computation and experiment for $100° \leq \phi \leq 150°$. This trend is accentuated for flow on the boattail.

Streamwise Velocity Profiles. A sensitive test of the accuracy of the PNS computational technique applied to this flow is the comparison of measured and computed boundary-layer velocity profiles. Such comparisons are shown in Figures 6 and 7 for two longitudinal stations; station A on the cylinder near the boattail, and station B on the boattail (Figure 3). Each figure shows the velocity profiles at a particular longitudinal station for circumferential stations completely around the model in 30° increments. The nondimensional streamwise velocity component, u, is plotted versus physical distance y measured radially from the body surface in millimeters, rather than against normalized y/δ. This method of plotting prevents scaling differences between the computation and experiment from giving a false comparison.

Comparisons for $M = 3$, $\alpha = 4.2°$ and a spin rate of 333 RPS are shown in Figures 6 and 7. The agreement is, in general, excellent. However, a slight discrepancy is visible for the profiles just off the lee-side at $\phi = 150°$ and 210°. This discrepancy, which is attributed to the formation of longitudinal

---

13. *Schiff, L. B., and Sturek, W. B. "Numerical Simulation of Steady Supersonic Flow Over an Ogive-Cylinder-Boattail Body", AIAA Paper No. 80-0066, 18th Aerospace Sciences Meeting, January 1980.*

vortices, becomes more pronounced at increased angles of attack and is discussed in more detail in Ref. 13. For the purpose of this study - which is to determine Magnus effects at small angle of attack - the agreement between computational and experimental velocity profiles is considered to be very satisfactory.

Magnus Force. The Magnus effect is strongly dependent on the circumferential pressure distributions and the asymmetries about the pitch plane that occur when the model is spinning. Thus the PNS technique is particularly attractive for computations of the Magnus effect since, as seen in Figures 4-5, the accuracy for the circumferential and longitudinal distributions of wall pressure are much improved over that obtained using inviscid techniques. This improvement was most significant for the flow over the boattail. In order to test the accuracy of the PNS code for computing Magnus effects, several test cases have been run for flow conditions where experimental measurements of Magnus forces and moments have been accomplished[11,12]. See Figure 8 for the sign convention used in evaluating the aerodynamic forces and moments.

The results of these computations for the 10° cone model are shown in Figure 9 and for the ogive-cylinder and ogive-cylinder-boattail models in Figures 10 and 11, respectively. The PNS computations are compared to inviscid-boundary layer results and to the experimental measurements as indicated. Tabulated results are presented in Tables 1, 2 and 3.

In Figures 9, 10 and 11, the individual components of the Magnus effect are plotted versus axial position for Mach = 3, $\alpha = 2°$, and $\Omega = 333$ RPS. Comparisons are shown of PNS and INV-BL results for the individual components of the Magnus effect. Excellent agreement for $C_{\tau\phi}$ (circumferential wall shear component) is indicated. Fair agreement is indicated for C_{pw} (wall pressure component of Magnus) between the two computational techniques. For the INV-BL technique, the component plotted as C_{pw} is the sum of the wall pressure and centrifugal pressure gradient contributions. This quantity is equivalent to the surface pressure contribution determined by the PNS code since the viscous and inviscid flow are computed simultaneously.

The lines in Figures 9-11 identified as C_Y represent the total Magnus effect. For the cone, both the PNS and INV-BL techniques achieve good agreement with the experiment. Considering the small magnitude of the Magnus force, the agreement with experiment shown in Figure 10 for the ogive-cylinder model is considered to be quite good for the INV-BL technique; however the PNS result is obviously better. This result is also considered to be verification of the INV-BL concept at small angle of attack. The results shown in Figure 11 show a dramatic superiority of the PNS technique compared to the INV-BL technique for the ogive-cylinder boattail model where the INV-BL technique greatly exaggerates the effect of the flow over the boattail.

Comparisons of the PNS computations to experiment for additional Mach number flow conditions ($2 \leq M \leq 4$) for the ogive-cylinder and ogive-cylinder-boattail models are shown for Magnus force coefficient in Figure 12 and for the slope of the Magnus moment coefficient in Figure 13. Excellent agreement is indicated for the Magnus force coefficient in Figure 12 for magnitude and

for trend with Mach number and body configuration. The agreement shown for the slope of the Magnus moment coefficient in Figure 13 is less satisfactory; however, the trend with Mach number and body configuration is accurately predicted. The absolute value of the prediction is well within that required for parametric design studies.

Computations have also been performed using the PNS code for laminar boundary layer flow over a 10° cone at $M = 4$, $\alpha = 2°$, $\Omega = 500$ RPS, $Tw/To = 0.24$. A constant wall temperature boundary condition was included in the PNS code for this computation. This is the case for which a reversed Magnus effect was reported in Ref. 5. The results of these computations are shown in Figures 14 and 15. Individual components of the side force coefficient due to the Magnus effect obtained with both computational methods are shown in Figure 14. The results differ considerably. In contrast to the results of Ref. 5, which show a reversal of the wall pressure component and total Magnus force with increasing body length, the present PNS results vary monotonically with body length. (Note that in Ref. 5 values of $C_{\tau x}$ and C_Y are given only at $x = 304.8$ mm (1.0 ft). The intermediate values shown in Figure 14 were obtained by assuming a linear variation of $C_{\tau x}$ with body length and summing the individual components $C_{\tau x}$, $C_{\tau \phi}$, and C_{pw} to obtain C_Y.) Additional computations were made for a wide range of grid configurations and the results evidenced no reversal of the Magnus force. The monotonic behavior of the present PNS results follows the classical trend, and is similar to that shown above for the turbulent case.

The results of an investigation of the effect of wall temperature is shown in Figure 15, where computations for a cold wall and adiabatic wall boundary conditions are compared. No tendency for a reversal of the Magnus force was obtained. The effect of the cold wall is to reduce the magnitude of the Magnus force.

C. Pitch Plane Aerodynamics

Examples of computed values for the slope of the pitching moment coefficient, C_{m_α}, and center of pressure, CP, are shown in Figures 16 and 17, respectively, compared to experiment for the ogive-cylinder and ogive-cylinder-boattail shapes. The agreement with experiment is excellent for the full range of Mach number, $2 \leq M \leq 4$.

IV. CONCLUDING REMARKS

A numerical computational study has been described in which the PNS marching code recently developed by Schiff and Steger has been used to compute Magnus effects for spinning, slender bodies. The PNS computations have been compared to INV-BL computations and to experimental measurements. The comparisons have shown that the PNS code yields excellent agreement with the experimental data. These results indicate that the PNS numerical technique, which

computes the inviscid flow and the viscous layer simultaneously, closely models the physics of the actual flow over the body including discontinuities in surface curvature. This feature has been shown to be of particular significance for computations of the flow over a boattailed afterbody.

The results also indicate verification of the suitability of the INV-BL technique for cone and ogive-cylinder bodies at small angle of attack in contradiction to a previous result for laminar viscous flow.

The comparisons of this paper represent the first comprehensive tests of PNS computations for turbulent, viscous flow over a spinning ogive-cylinder-boattail model and indicate that the PNS code reported here represents a viable computational tool for predicting Magnus effects for spinning projectiles at small angle of attack.

REFERENCES

1. Sturek, W.B., Dwyer, H.A., Kayser, L.D., Nietubicz, C.J., Reklis, R.P., and Opalka, K.O., "Computations of Magnus Effects for a Yawed, Spinning Body of Revolution," AIAA Journal, Vol. 16, No. 7, July 1978, pp. 687-692.

2. Lin, T. C., and Rubin, S. G., "Viscous Flow Over a Cone at Moderate Incidence: I Hypersonic Tip Region," Computers and Fluids, Vol. 1, 1973, pp. 37-57.

3. Lubard, S. C., and Helliwell, W. S., "Calculation of the Flow on a Cone at High Angle of Attack," AIAA Journal, Vol. 12, July 1974, pp. 965-974.

4. Rakich, J. V., Vigneron, Y. C., and Agarwal, R., "Computation of Supersonic Viscous Flows Over Ogive-Cylinders at Angle of Attack," AIAA Paper No. 79-0131, 17th Aerospace Sciences Meeting, January 1979.

5. Agarwal, R., and Rakich, J. V., "Computation of Hypersonic Laminar Viscous Flow Past Spinning Sharp and Blunt Cones at High Angle of Attack," AIAA Paper No. 78-65, 16th Aerospace Sciences Meeting, January 1978.

6. Schiff, L. B., and Steger, J. L., "Numerical Simulation of Steady Supersonic Viscous Flow," AIAA Journal, Vol. 18, No. 12, December 1980, pp. 1421-1430.

7. Baldwin, B. S., and Lomax, H., "Thin Layer Approximation and Algebraic Model for Separated Turbulent Flows," AIAA Paper No. 78-257, 16th Aerospace Sciences Meeting, January 1978.

8. Reklis, R. P., and Sturek, W. B., "Surface Pressure Measurements on Slender Bodies at Angle of Attack in Supersonic Flow,"U.S. Army Ballistic Research Laboratory/ARRADCOM Memorandum Report ARBRL-MR-02876, Aberdeen Proving Ground, MD, November 1978. AD A064097.

9. Kayser, L. D., and Sturek, W. B., "Experimental Measurements in the Turbulent Boundary Layer of a Yawed, Spinning Ogive-Cylinder Body of Revolution at Mach 3.0. Part II: Data Tabulation,"U.S. Army Ballistic Research Laboratory/ARRADCOM Memorandum Report ARBRL-MR-02813, Aberdeen Proving Ground, MD, March 1978. AD A053458.

10. Kayser, L. D., and Sturek, W. B., "Turbulent Boundary Layer Measurements on the Boattail Section of a Yawed, Spinning Projectile Shape at Mach 3.0," U.S. Army Ballistic Research Laboratory/ARRADCOM Memorandum Report ARBRL-MR-02880, Aberdeen Proving Ground, MD, November 1978. AD A065355.

11. Sturek, W. B., "Boundary Layer Studies on a Spinning Cone," U.S. Army Ballistic Research Laboratory/ARRADCOM Report BRL-R-1649, Aberdeen Proving Ground, MD, May 1973. AD 762564.

REFERENCES
(Continued)

12. Nietubicz, C. J., and Opalka, K., "Supersonic Wind Tunnel Measurements of Static and Magnus Aerodynamic Coefficients for Projectile Shapes with Tangent and Secant Ogive Noses," U.S. Army Ballistic Research Laboratory/ ARRADCOM Memorandum Report ARBRL-MR-02991, Aberdeen Proving Ground, MD, February 1980. AD A083297.

13. Schiff, L. B., and Sturek, W. B., "Numerical Simulation of Steady Supersonic Flow Over an Ogive-Cylinder-Boattail Body," AIAA Paper No. 80-0066, 18th Aerospace Sciences Meeting, January 1980.

Table 1. Magnus Force Components for 10° Cone;
$M = 3$, $\alpha = 2°$, $\Omega = 333$ RPS

	$C_{\tau x}$	$C_{\tau \phi}$	$C_{\Delta p}$	C_{pw}	C_Y
PNS	$-.769 \times 10^{-6}$	$.772 \times 10^{-4}$	$-.933 \times 10^{-7}$	$-.244 \times 10^{-3}$	$-.168 \times 10^{-3}$
INV-BL	$.636 \times 10^{-6}$	$.792 \times 10^{-4}$	$-.170 \times 10^{-3}$	$-.108 \times 10^{-3}$	$-.198 \times 10^{-3}$
EXP					$-.170 \times 10^{-3}$

Table 2. Magnus Force Components for Ogive-Cylinder Body;
$M = 3$, $\alpha = 2°$, $\Omega = 333$ RPS

	$C_{\tau x}$	$C_{\tau \phi}$	$C_{\Delta p}$	C_{pw}	C_Y
PNS	$-.102 \times 10^{-5}$	$.215 \times 10^{-3}$	$-.842 \times 10^{-6}$	$-.253 \times 10^{-2}$	$-.00232$
INV-BL	$.570 \times 10^{-6}$	$.197 \times 10^{-3}$	$-.161 \times 10^{-2}$	$-.242 \times 10^{-2}$	$-.00383$
EXP					$-.00250$

Table 3. Magnus Force Components for Ogive-Cylinder-Boattail Body;
$M = 3$, $\alpha = 2°$, $\Omega = 333$ RPS

	$C_{\tau x}$	$C_{\tau \phi}$	$C_{\Delta p}$	C_{pw}	C_Y
PNS	$-.147 \times 10^{-5}$	$.180 \times 10^{-3}$	$-.801 \times 10^{-6}$	$-.278 \times 10^{-2}$	$-.00259$
INV-BL	$.225 \times 10^{-5}$	$.175 \times 10^{-3}$	$-.190 \times 10^{-2}$	$-.427 \times 10^{-2}$	$-.00599$
EXP					$-.00300$

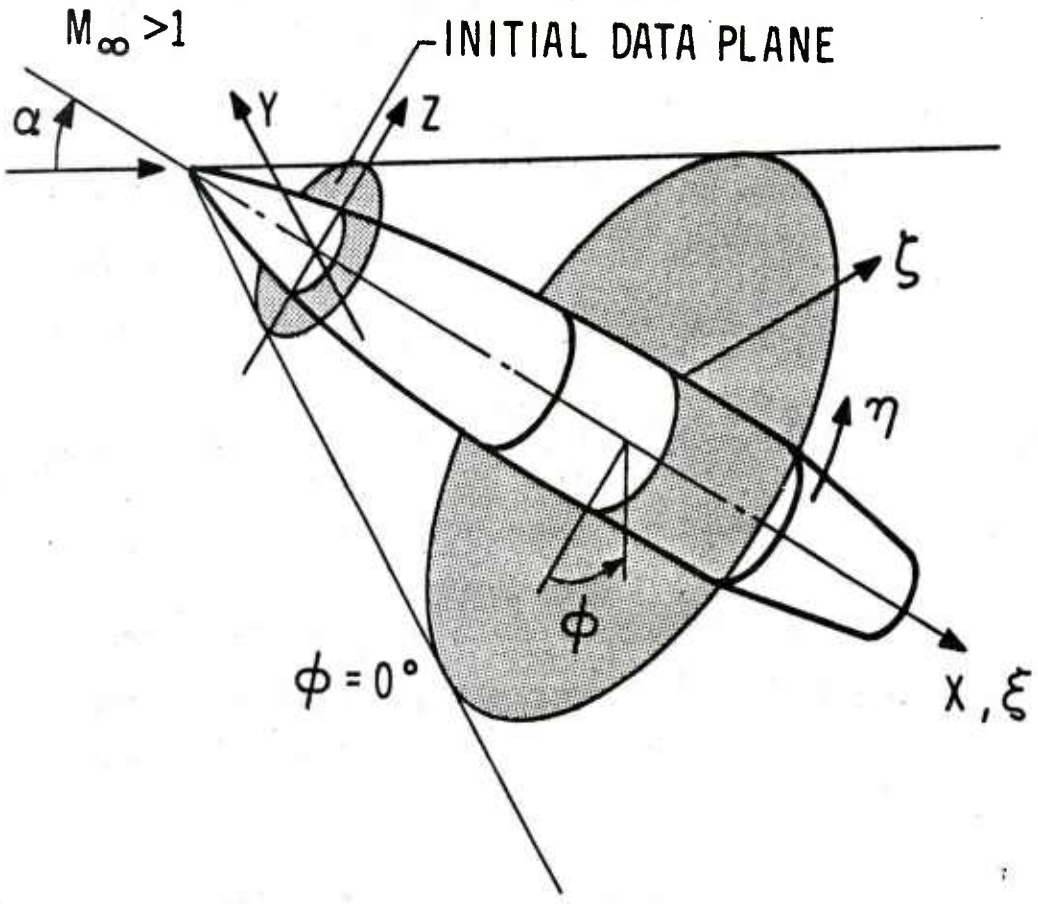

Figure 1. Coordinates and Notation

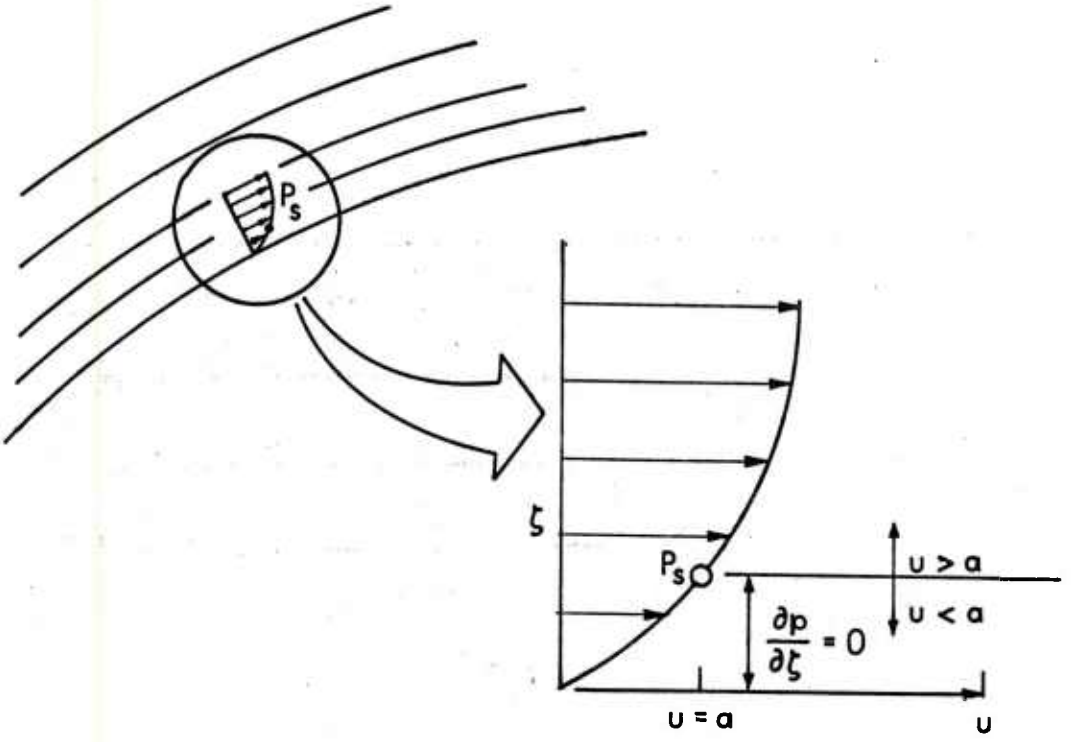

Figure 2. Subsonic Layer Approximation

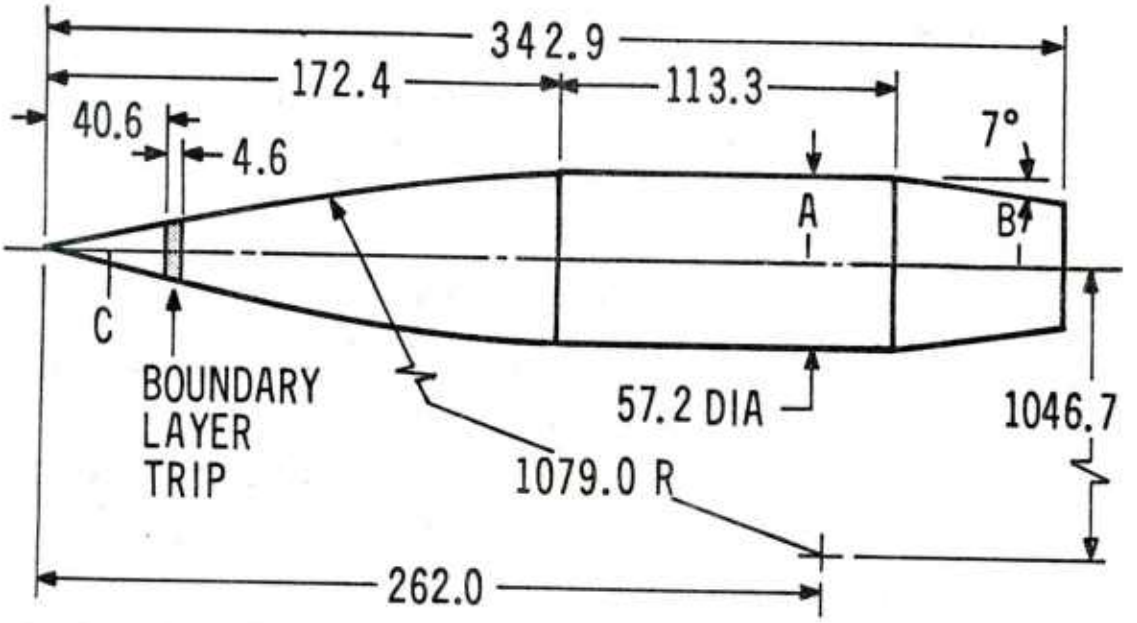

NOTE: DIMENSIONS ARE IN MILLIMETRES
A,B BOUNDARY LAYER SURVEY STATIONS
C CONICAL STARTING SOLUTION STATION

Figure 3. Model Configuration for Detailed Flow Field Studies

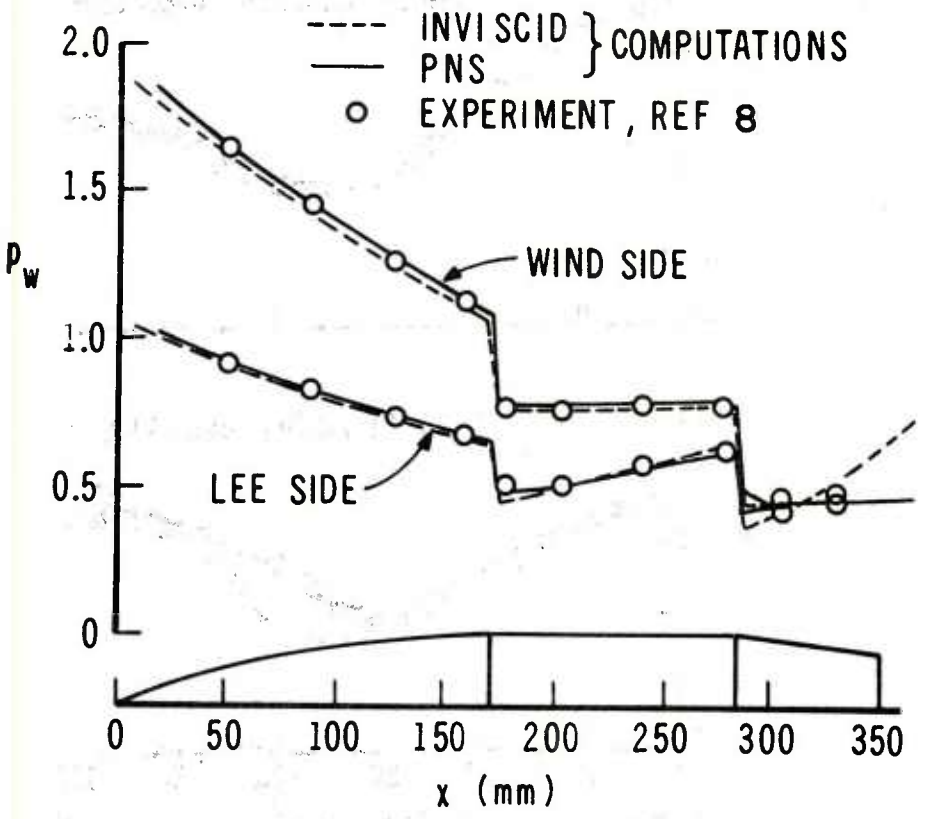

Figure 4. Axial Surface Pressure Distribution for Ogive-Cylinder-Boattail Body; $M = 3$, $\alpha = 6.3°$, $\Omega = 0$ RPS, $Re = 2.13 \times 10^7/m$

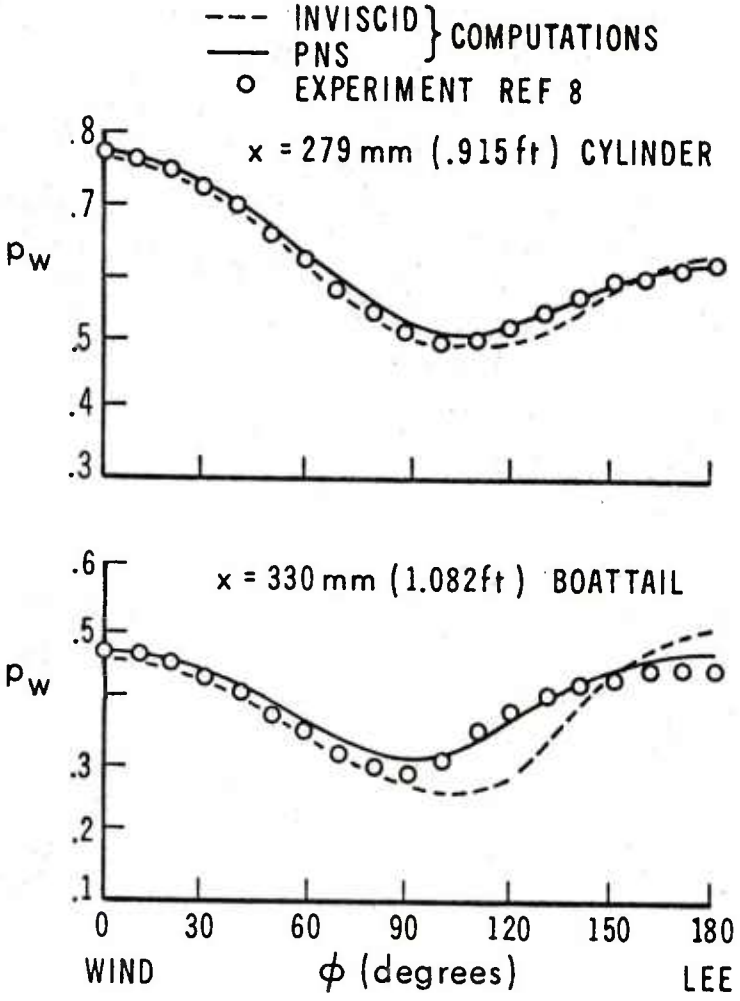

Figure 5. Circumferential Surface Pressure Distributions for Ogive-Cylinder-Boattail Body; M = 3, α = 6.3°, Ω = 0 RPS, Re = 2.13 × 10^7/m

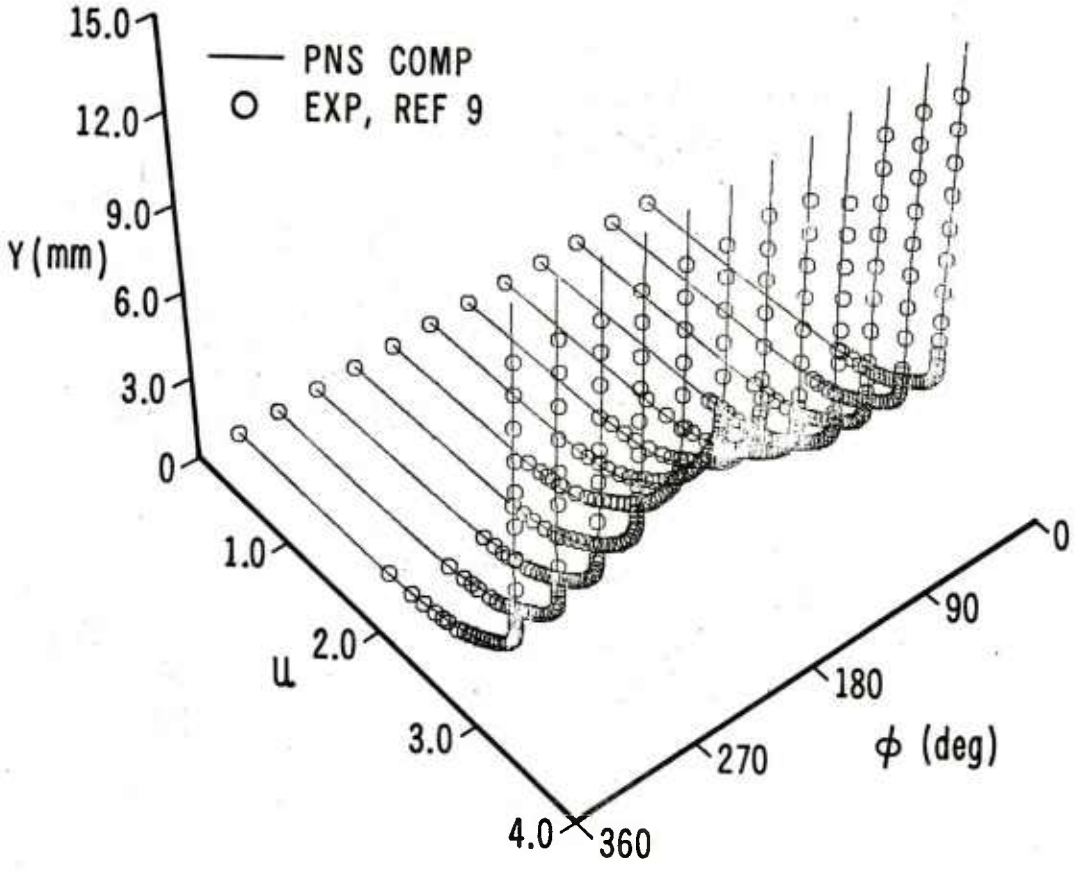

Figure 6. Boundary-Layer Velocity Profiles for Ogive-Cylinder-Boattail Body; M = 3, α = 4.2°, Ω = 333 RPS, Re = 2.13 × 10^7/m, x = 254mm, Cylinder

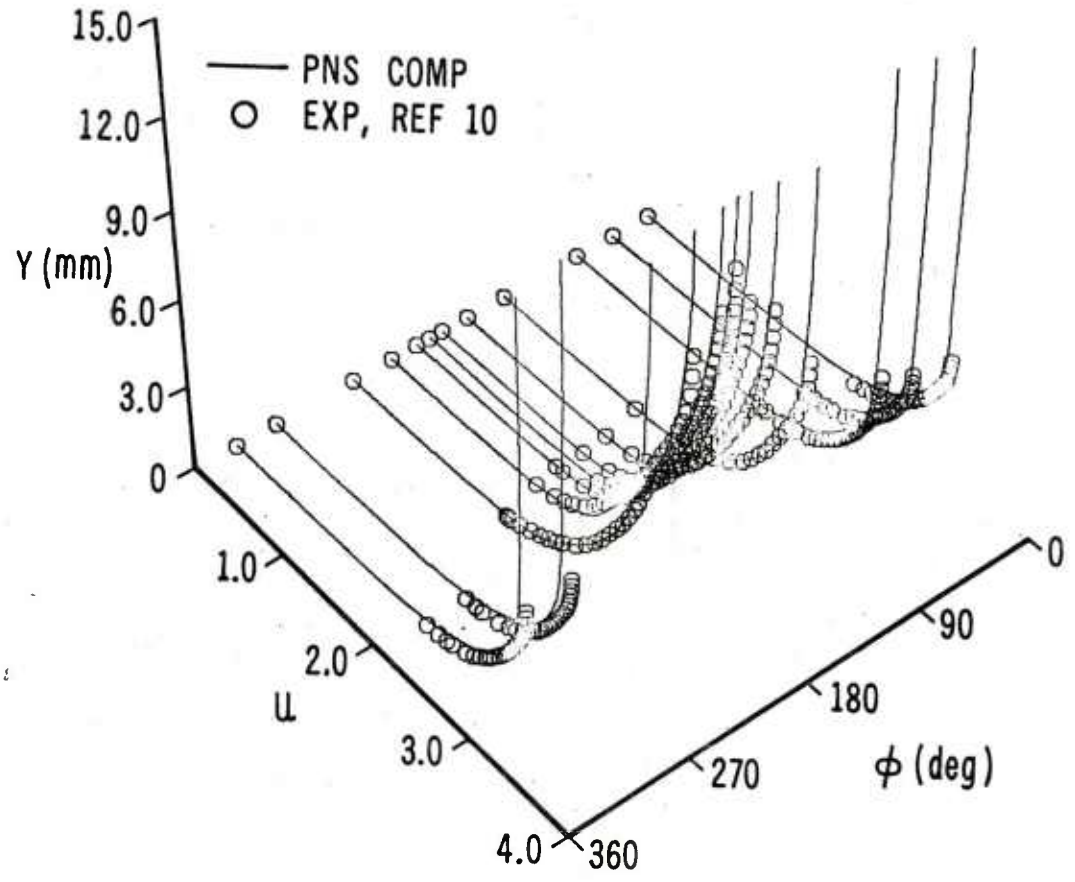

Figure 7. Boundary-Layer Velocity Profiles for Ogive-Cylinder-Boattail Body; M = 3, α = 4.2°, Ω = 333 RPS, Re = 2.13 × 10^7/m, x = 324mm, Boattail

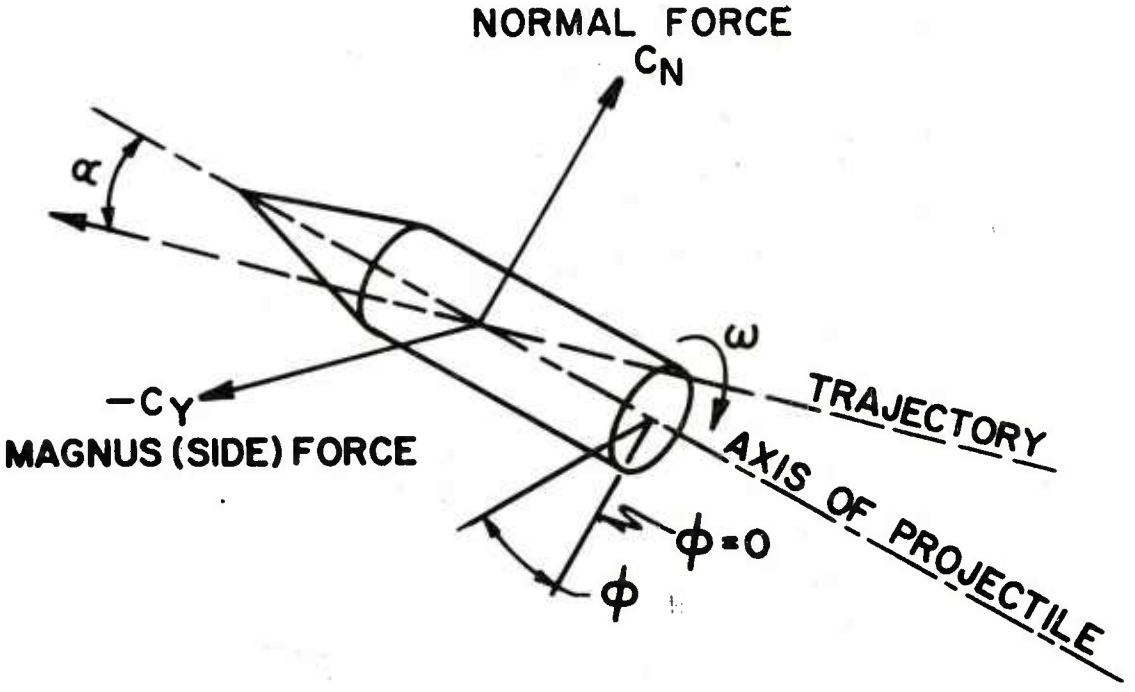

Figure 8. Sign Convention for Aerodynamic Forces

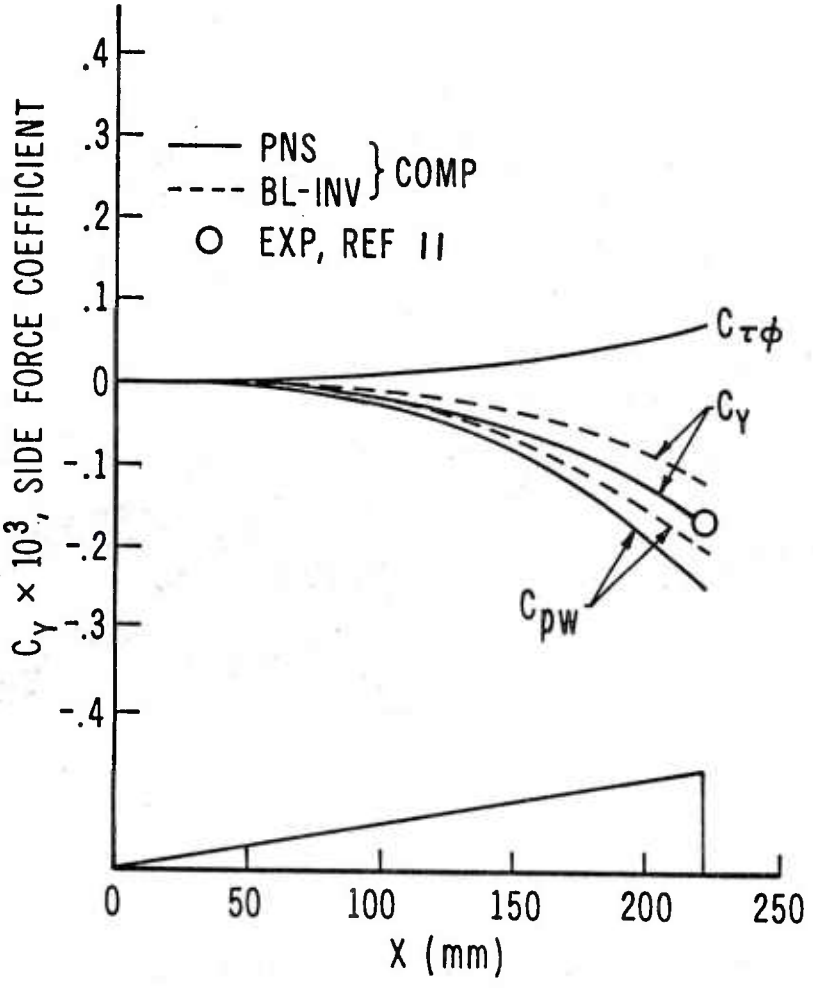

Figure 9. Magnus Force Coefficient for 10° Cone; M = 3, α = 2°, Ω = 333 RPS, Re = 2.352 × 10^7/m, Turbulent Boundary-Layer

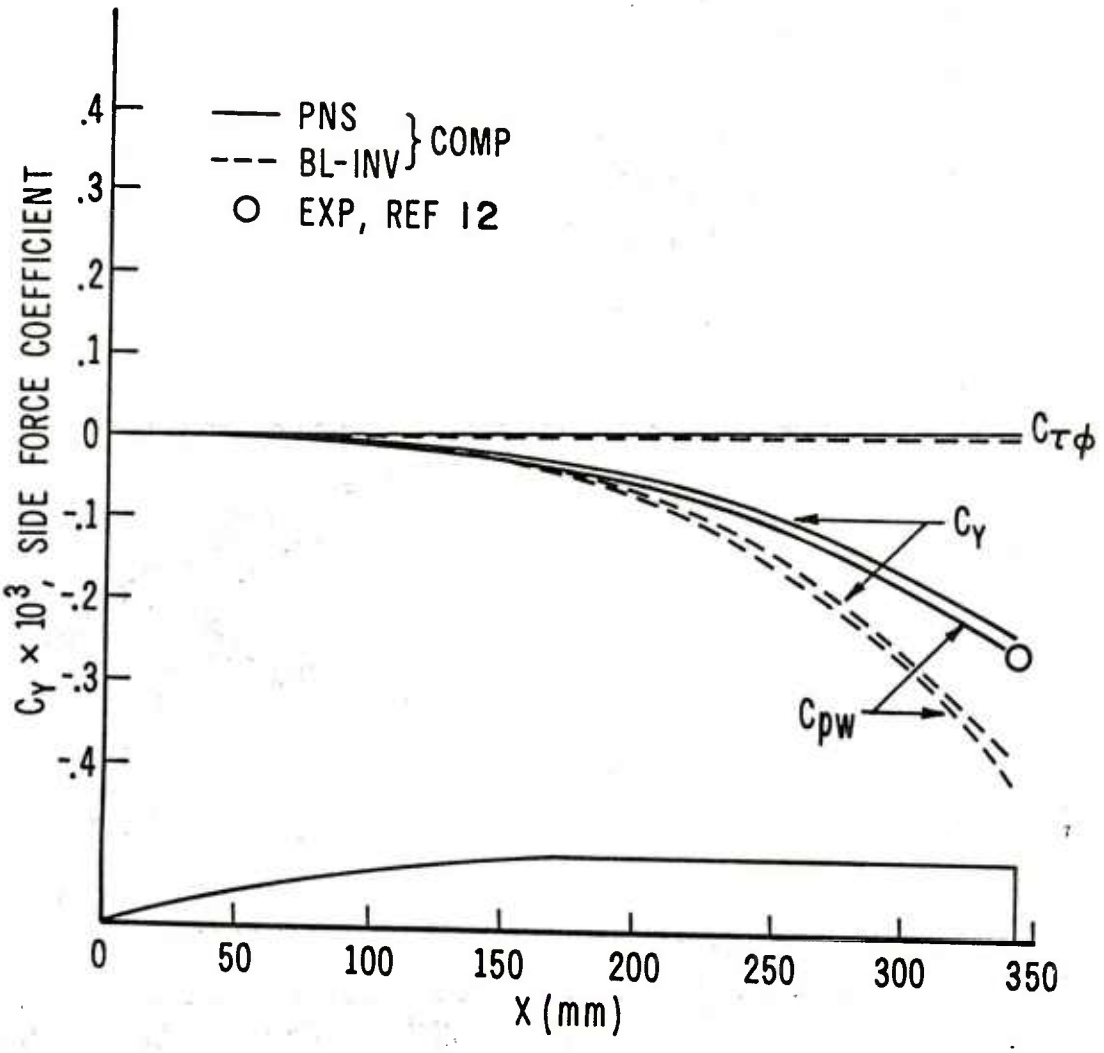

Figure 10. Magnus Force Coefficient for Ogive-Cylinder Body; M = 3, α = 2°, Ω = 333 RPS, Re = 2.11 × 10^7/m, Turbulent Boundary-Layer

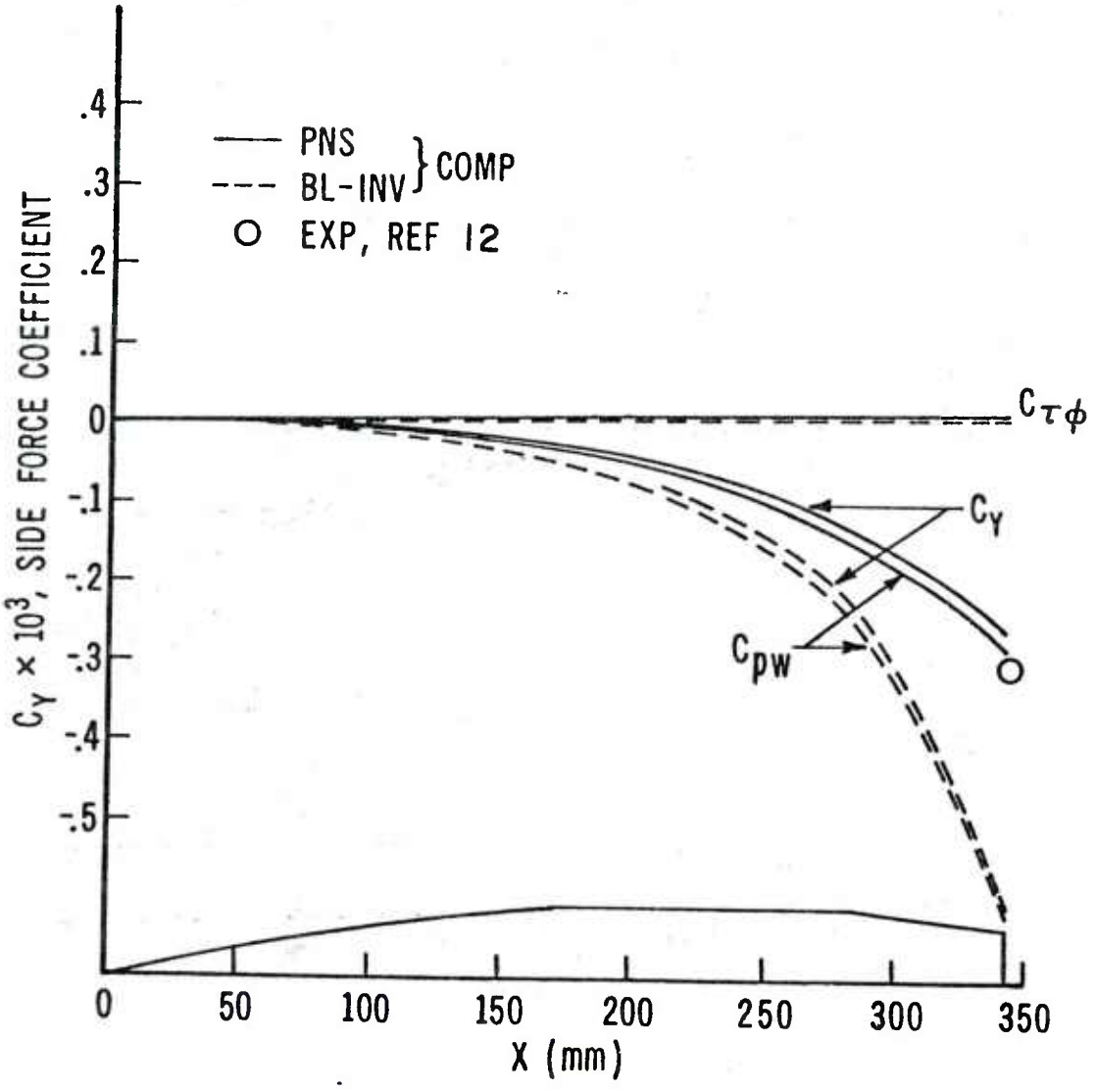

Figure 11. Magnus Force Coefficient for Ogive-Cylinder-Boattail Body; M = 3, α = 2°, Ω = 333 RPS, Re = 2.11 × 10^7/m, Turbulent Boundary-Layer

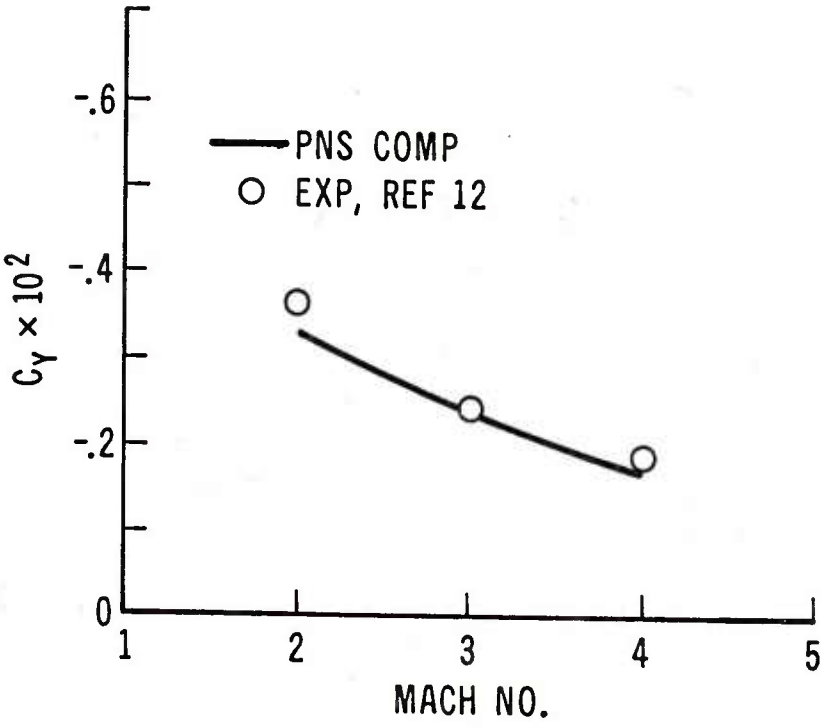

Figure 12a. Magnus Force Coefficient for Ogive-Cylinder Body; $\alpha = 2°$, $\Omega = 333$ RPS, Turbulent Boundary Layer

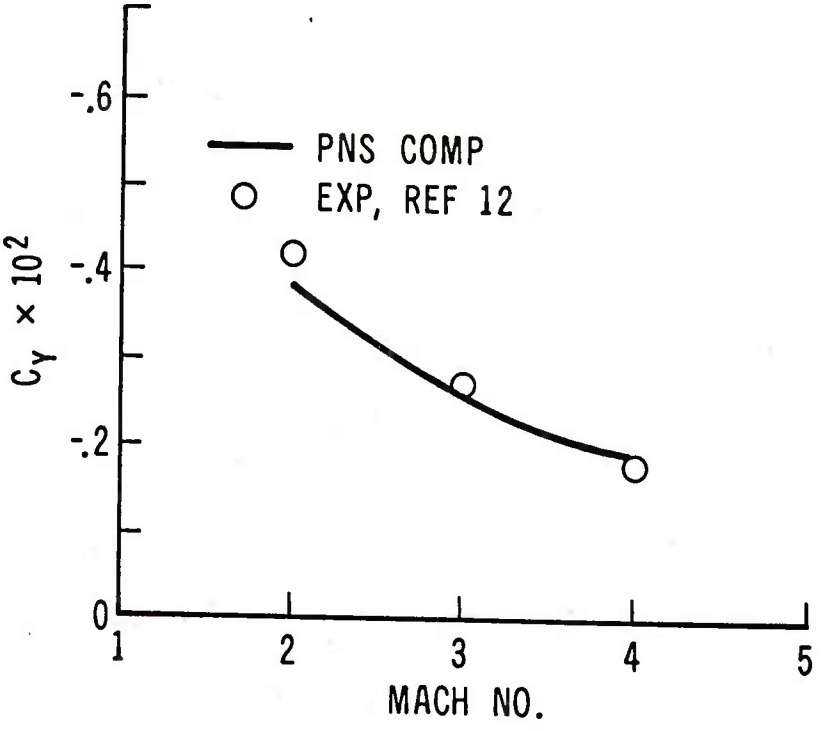

Figure 12b. Magnus Force Coefficient for Ogive-Cylinder-Boattail Body; $\alpha = 2°$, $\Omega = 333$ RPS, Turbulent Boundary-Layer

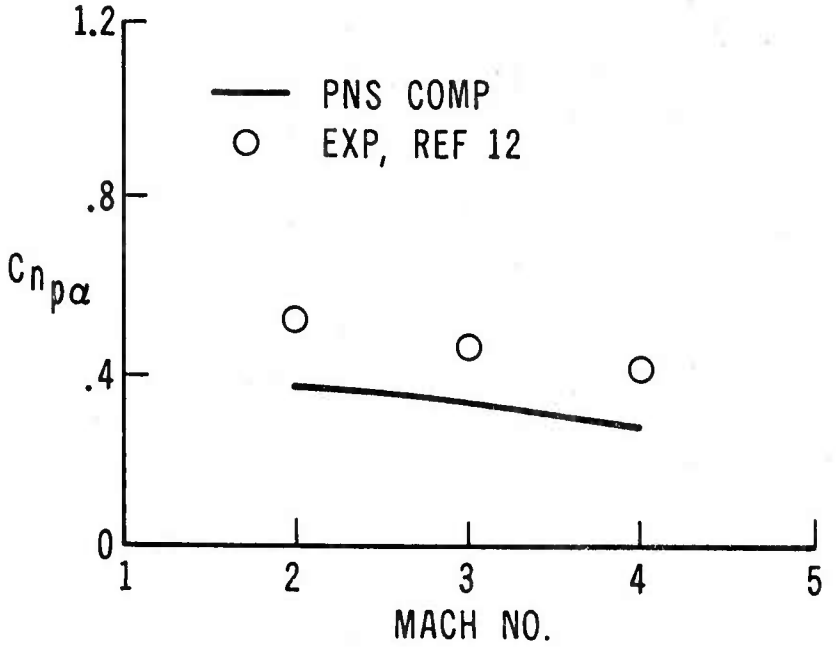

Figure 13a. Magnus Moment Coefficient for Ogive-Cylinder Body; Turbulent Boundary Layer

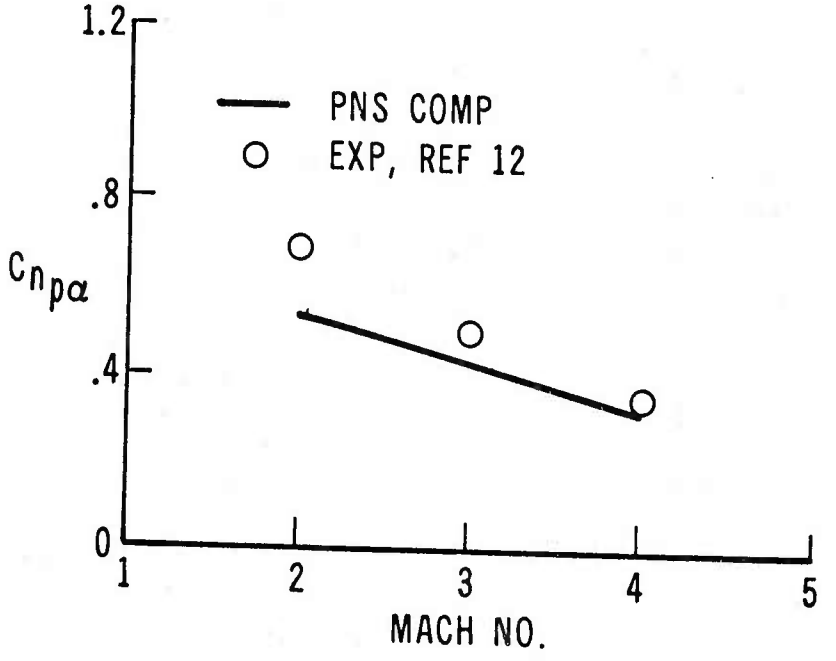

Figure 13b. Magnus Moment Coefficient for Ogive-Cylinder-Boattail Body; Turbulent Boundary-Layer

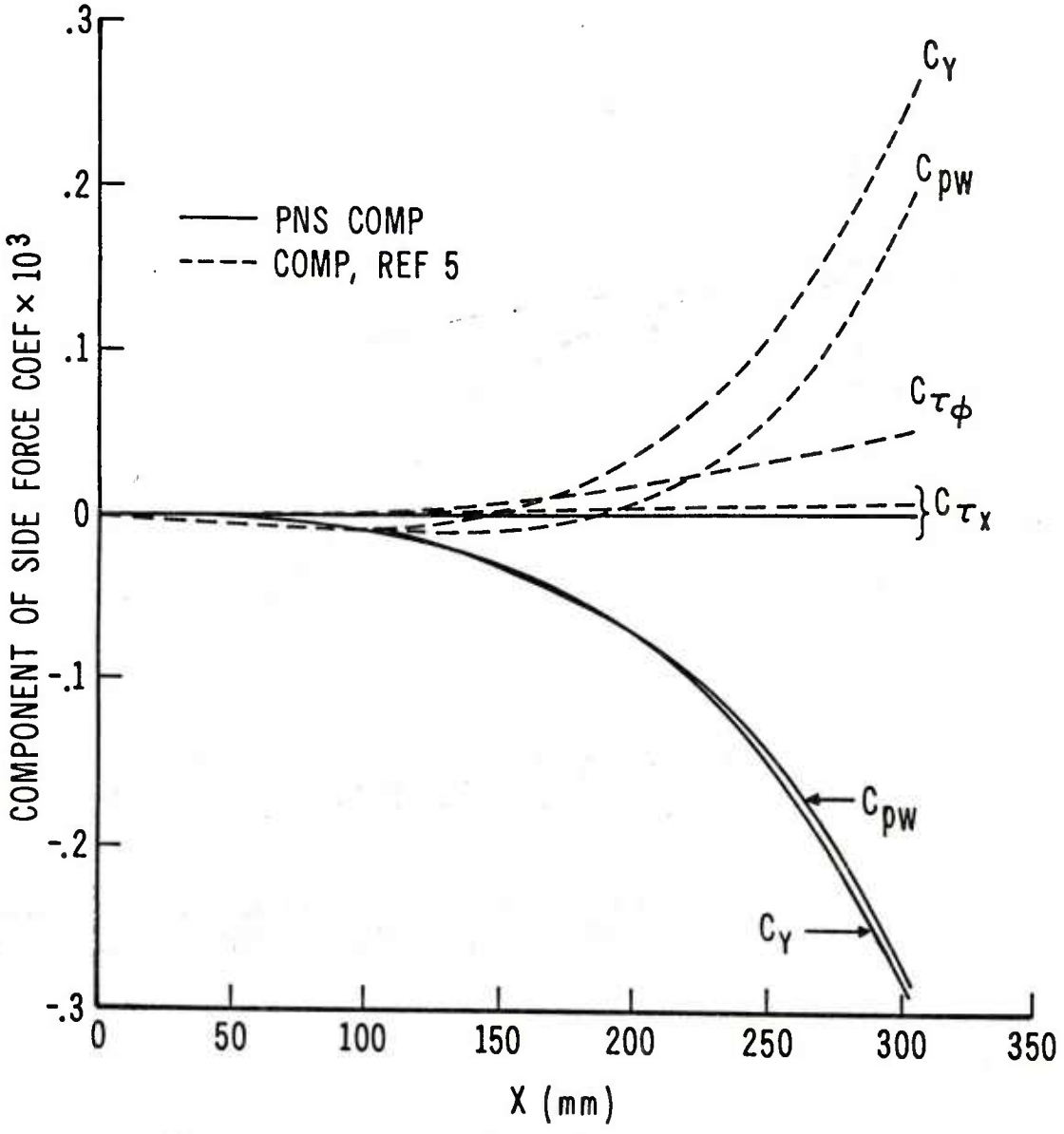

Figure 14. Magnus Force Coefficient for 10° Cone; M = 4, α = 2°, Ω = 500 RPS, Tw/To = 0.24, Re = 9.22 × 10^6/m, Laminar Boundary-Layer

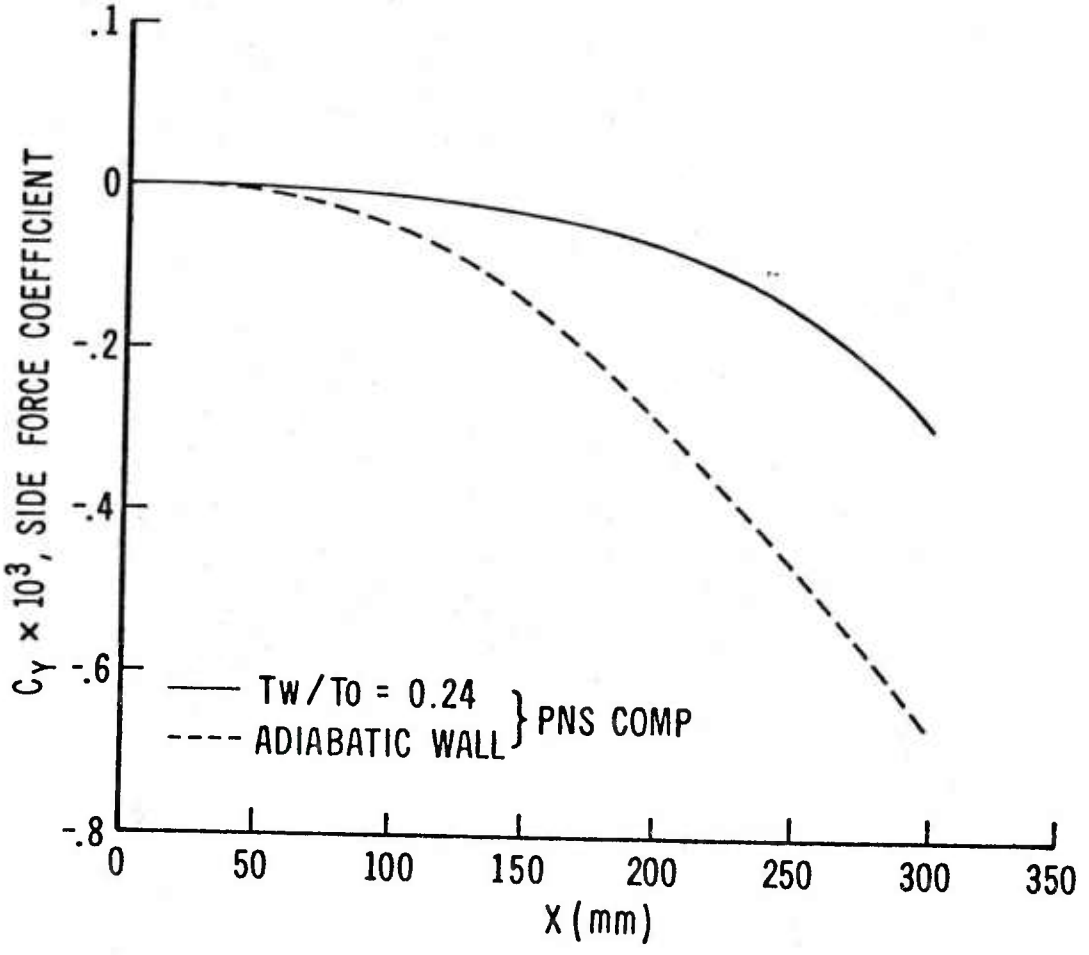

Figure 15. Magnus Force Coefficient for 10° Cone; M = 4, α = 2°, Ω = 500 RPS, Re = 9.22 × 10^6/m, Laminar Boundary-Layer

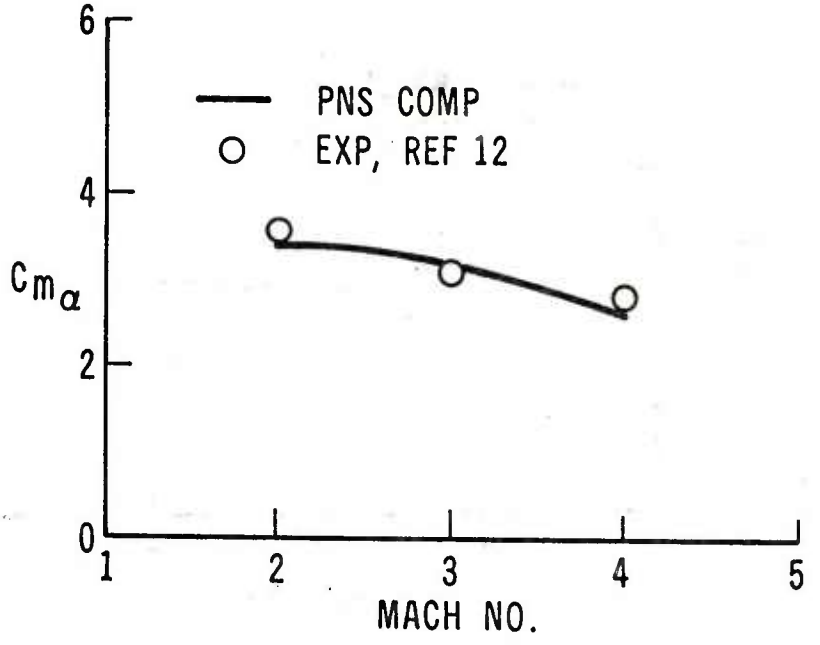

Figuer 16a. Pitching Moment Coefficient for Ogive-Cylinder Body; Turbulent Boundary-Layer

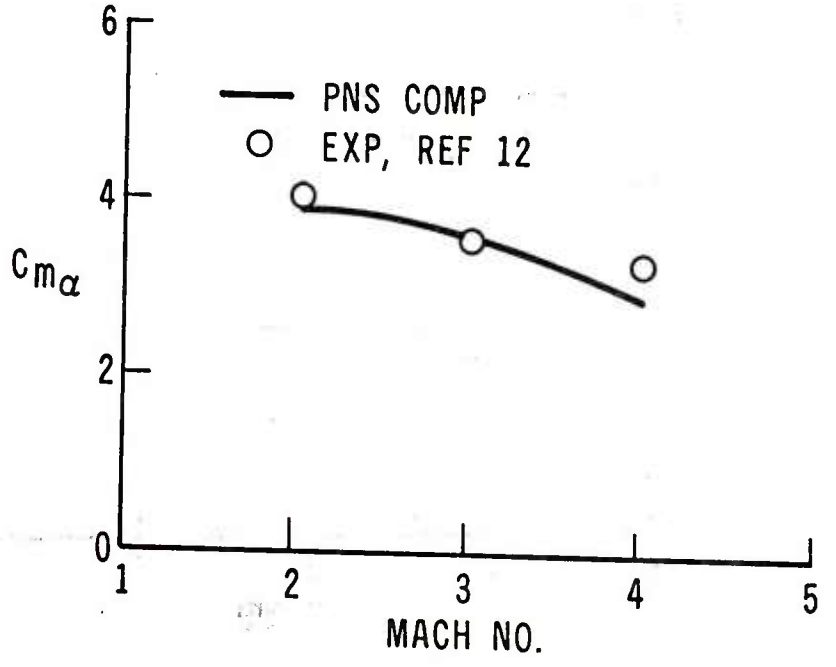

Figure 16b. Pitching Moment Coefficient for Ogive-Cylinder-Boattail Body; Turbulent Boundary-Layer

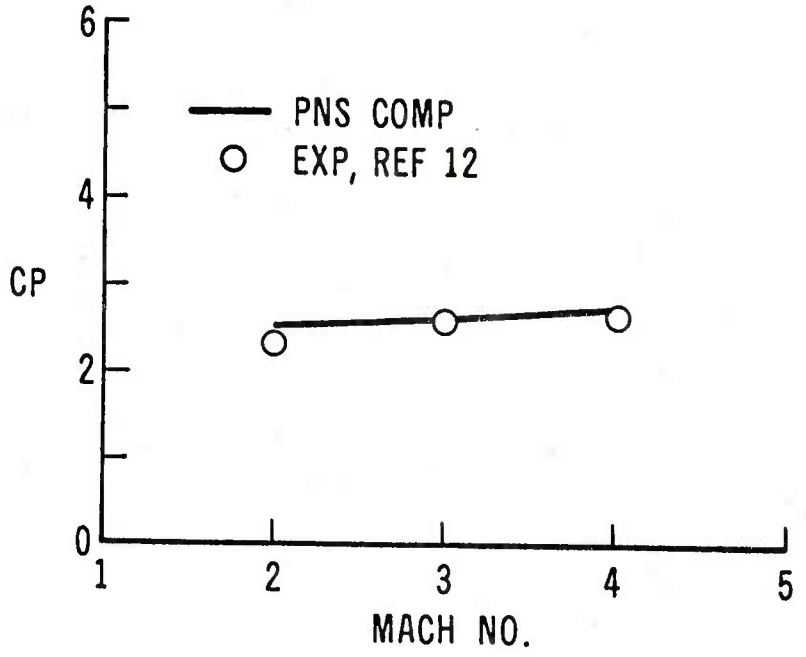

Figure 17a. Center of Pressure for Ogive-Cylinder Body; Turbulent Boundary-Layer

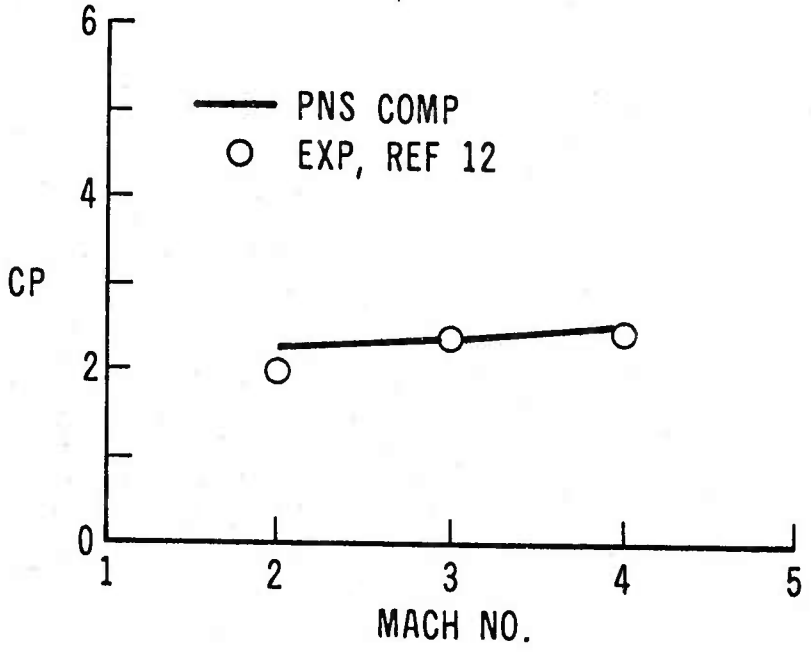

Figure 17b. Center of Pressure for Ogive-Cylinder-Boattail Body; Turbulent Boundary-Layer

LIST OF SYMBOLS

a	speed of sound
c_p	specific heat at constant pressure
CP	center of pressure for normal force
C_m	pitching moment coefficient
C_{m_α}	$dC_m/d\alpha$, slope of pitching moment coefficient evaluated at $\alpha = 0$
C_n	Magnus (yawing) moment coefficient
$C_{n_{p\alpha}}$	$d^2C_n/[d(\frac{PD}{V})\cdot d\alpha]$, slope of Magnus moment coefficient evaluated at $\Omega = 0$, $\alpha = 0$
C_Y	Magnus (side) force coefficient
C_{pw}	wall surface pressure component of Magnus force coefficient
$C_{\Delta p}$	centrifugal pressure gradient component of Magnus force coefficient
$C_{\tau x}$	longitudinal velocity wall shear component of Magnus force coefficient
$C_{\tau\phi}$	circumferential velocity wall shear component of Magnus force coefficient
D	diameter of model
e	total energy per unit volume of fluid, normalized by $\rho_\infty a_\infty^2$
e_i	internal energy, normalized by a_∞^2
$\hat{E}_s,\hat{F},\hat{G},\hat{q}$	flux vectors of transformed gasdynamic equation (Eq. 2)
J	Jacobian of transformation between physical and computational coordinates
L	reference length
M	Mach number
p	pressure, normalized by $\rho_\infty a_\infty^2$
Pr	Prandtl number, $\mu_\infty c_p/\kappa_\infty$
Re	Reynolds number, $\rho_\infty U_\infty L/\mu_\infty$
$\hat{Re}$	Reynolds number (Eq. 1), $\rho_\infty a_\infty L/\mu_\infty$

LIST OF SYMBOLS
(Continued)

$\hat{S}$	viscous flux vector (Eq. 6)
u,v,w	Cartesian velocity components along the x, y, z axis, respectively, normalized by a_∞
U,V,W	contravariant velocity components (Eq. 3)
x,y,z	physical Cartesian coordinate axes (Fig. 1)
α	angle of attack
γ	ratio of specific heats
κ	coefficient of thermal conductivity, normalized by free-stream value κ_∞
μ	coefficient of viscosity, normalized by free-stream value μ_∞
ξ,η,ζ	computational coordinates in the axial, circumferential, and radial directions (Fig. 1)
ρ	density, normalized by free-stream density ρ_∞
ϕ	circumferential angle (Figure 1)
Ω	spin rate about body axis, RPS

Subscripts

∞	free-stream conditions
w	body surface values
x	based on axial distance from nose

DISTRIBUTION LIST

No. of Copies	Organization
12	Commander Defense Technical Info Center ATTN: DDC-DDA Cameron Station Alexandria, VA 22314
1	Commander US Army Materiel Development and Readiness Command ATTN: DRCDMD-ST 5001 Eisenhower Avenue Alexandria, VA 22333
9	Commander US Army Armament Research and Development Command ATTN: DRDAR-TSS (2 cys) DRDAR-LCA-F Mr. D. Mertz Mr. E. Falkowski Mr. A. Loeb Mr. R. Kline Mr. S. Kahn Mr. S. Wasserman Mr. H. Hudgins Dover, NJ 07801
1	Commander US Army Armament Materiel Readiness Command ATTN: DRSAR-LEP-L, Tech Lib Rock Island, IL 61299
1	Director US Army Armament Research and Development Command Benet Weapons Laboratory ATTN: DRDAR-LCB-TL Watervliet, NY 12189
1	Commander US Army Aviation Research and Development Command ATTN: DRDAV-E 4300 Goodfellow Boulevard St. Louis, MO 63120
1	Director US Army Air Mobility Research and Development Laboratory Ames Research Center Moffett Field, CA 94035
1	Commander US Army Communications Research and Development Command ATTN: DRDCO-PPA-SA Fort Monmouth, NJ 07703
1	Commander US Army Electronics Research and Development Command Technical Support Activity ATTN: DELSD-L Fort Monmouth, NJ 07703
2	Commander US Army Missile Command ATTN: DRSMI-R DRSMI-RDK Mr. R. Deep Redstone Arsenal, AL 35809
1	Commander US Army Missile Command ATTN: DRSMI-YDL Redstone Arsenal, AL 35809
1	Commander US Army Tank Automotive Research and Development Command ATTN: DRDTA-UL Warren, MI 48090
1	Director US Army TRADOC Systems Analysis Activity ATTN: ATAA-SL, Tech Lib White Sands Missile Range, NM 88002

DISTRIBUTION LIST

No. of Copies	Organization
1	Commander US Army Research Office P. O. Box 12211 Research Triangle Park NC 27709
1	Commander US Naval Air Systems Command ATTN: AIR-604 Washington, D. C. 20360
2	Commander David W. Taylor Naval Ship Research and Development Center ATTN: Dr. S. de los Santos Mr. Stanley Gottlieb Bethesda, Maryland 20084
4	Commander US Naval Surface Weapons Center ATTN: Dr. T. Clare, Code DK20 Mr. P. Daniels Mr. D. A. Jones III Mr. L. Mason Dahlgren, VA 22448
5	Commander US Naval Surface Weapons Center ATTN: Code 312 Dr. C. Shieh Dr. W. Yanta Mr. R. Voisint Silver Spring, MD 20910
1	Commander US Naval Weapons Center ATTN: Code 3431, Tech Lib China Lake, CA 93555
1	Director NASA Langley Research Center ATTN: NS-185, Tech Lib Langley Station Hampton, VA 23365
1	Director NASA Ames Research Center ATTN: MS-227-8 Dr. L. Schiff Moffett Field, CA 94035
1	Nielsen Engineering & Research, Inc. ATTN: Dr. S. Stahara 510 Clyde Avenue Mountain View, CA 94043
3	Sandia Laboratories ATTN: Technical Staff, Dr. W.L. Oberkampf Aeroballistics Division 5631, G.R. Eisner H.R. Vaughn Albuquerque, NJ 87184
1	Massachusetts Institute of Technology ATTN: Tech Library 77 Massachusetts Avenue Cambridge, MA 02139
1	Stanford University Department of Aeronautics and Astronautics ATTN: Prof. J. Steger Stanford, CA 94305
1	University of California, Davis Department of Mechanical Engineering ATTN: Prof. H.A. Dwyer Davis, CA 95616
1	University of Colorado Department of Aerospace Engineering ATTN: Prof. G. Inger Boulder, CO 80309

DISTRIBUTION LIST

No. of Copies	Organization
1	University of Delaware Mechanical and Aerospace Engineering Department ATTN: Dr. J. E. Danberg Newark, DE 19711
1	University of Florida ATTN: Dr. J.E. Milton P.O. Box 1918 Eglin AFB, FL 32542

Aberdeen Proving Ground

Dir, USAMSAA
ATTN: DRXSY-D
DRXSY-MP, H. Cohen

Cdr, USATECOM
ATTN: DRSTE-TO-F

Dir, USACSL, Bldg. E3516, EA
ATTN: DRDAR-CLB-PA

USER EVALUATION OF REPORT

Please take a few minutes to answer the questions below; tear out this sheet, fold as indicated, staple or tape closed, and place in the mail. Your comments will provide us with information for improving future reports.

1. BRL Report Number _____

2. Does this report satisfy a need? (Comment on purpose, related project, or other area of interest for which report will be used.)

_____

_____

_____

3. How, specifically, is the report being used? (Information source, design data or procedure, management procedure, source of ideas, etc.) _____

_____

_____

4. Has the information in this report led to any quantitative savings as far as man-hours/contract dollars saved, operating costs avoided, efficiencies achieved, etc.? If so, please elaborate.

_____

_____

5. General Comments (Indicate what you think should be changed to make this report and future reports of this type more responsive to your needs, more usable, improve readability, etc.) _____

_____

_____

_____

6. If you would like to be contacted by the personnel who prepared this report to raise specific questions or discuss the topic, please fill in the following information.

Name: _____

Telephone Number: _____

Organization Address: _____

_____

_____